Analyzing and Monitoring the Impact of Streamflow Drought on Hydroelectricity Production: A Global-Scale Study

Wenhua Wan [1], Jianshi Zhao [1], Eklavyya Popat [2], Claudia Herbert [2], Petra Döll [2,3]

[1] State Key Laboratory of Hydro-science and Engineering, Department of Hydraulic Engineering, Tsinghua University, Beijing, China

[2] Institute of Physical Geography, Goethe University Frankfurt, Frankfurt am Main, Germany

[3] Senckenberg Leibniz Biodiversity and Climate Research Centre Frankfurt (SBiK-F), Frankfurt am Main, Germany

Correspondence to: P. Döll, p.doell@em.uni-frankfurt.de

Key Points:

- A new global hydropower database and a hydroelectricity production model have been developed and validated.
- The model simulates the impact of streamflow drought on hydroelectricity production worldwide.
- We suggest four indices of hydroelectricity production decrease that can be included in near-real-time drought monitoring.

Abstract

Electricity production by hydropower is negatively affected by drought. To understand, monitor and manage risks of less than normal streamflow for hydroelectricity production (HP) at the global scale, we developed an HP model that simulates time series of monthly HP worldwide and thus enables analyzing and monitoring the impact of drought on HP. The HP model is based on a new global hydropower database (GHD), containing 8748 geo-localized plant records, and on monthly streamflow values computed by the global hydrological model WaterGAP. The GHD includes 43 attributes and covers 91.8% of the globally installed capacity. The HP model can capture the interannual variability of country-scale HP that was caused by both (de)commissioning of hydropower plants and streamflow variability. It can also simulate the streamflow drought and its impact on HP reasonably well. A drought risk analysis for period 1975−2016 revealed the reduction of HP that is exceeded in 1 out of 10 years. 71 out of 134 countries with hydropower suffer from a reduction of more than 20% of average HP, and 20 countries from a reduction of more than 40%. We suggest four indices for monitoring the drought impact on HP in grid cells and on total electricity production in countries. These indices quantify the impact in terms of either relative reduction or anomaly. Applying the developed HP model, these indices can be included in global drought monitoring systems and inform stakeholders such as hydropower producer and national energy agencies about the reduced energy production due to streamflow drought.

1 Introduction

Electricity production by hydropower plants harnesses the energy of flowing water, a renewable source for electricity production. In case of most hydropower plants, greenhouse gas emissions per kW of generated electricity, mainly caused by methane emissions from reservoirs behind hydropower dams, are much smaller than emissions caused by fossil fuel-based electricity production (IHA, 2018). Hydroelectricity production (HP) continuously increased from 1296 TWh in 1973 to 4170 TWh in 2016 (IEA, 2019). In 2016, HP accounted for 16.3% of the worldwide gross electricity production and for 67.1% of all renewable electricity production, while it is expected to increase by 2.5%/yr through 2030 (IEA, 2019). In 2017, installed hydropower capacity was increased by 1.7%, almost half of it in China. Even though ecological impacts of large and small hydropower production can be considerable (e.g. Benejam et al., 2016; Bunn & Arthington, 2002), expansion of hydropower production may be suitable for providing electricity, in particular in least developed and electricity-poor countries (UNCTAD, 2017).

In hydropower plants, water is led through pipes from a location (e.g. upstream reservoir) at a higher elevation to a location (e.g. tail water) at a lower elevation; the flowing water causes rotation of turbines that generators convert mechanical energy into electricity. HP is a function of the product of elevation difference (hydraulic head) and water flow, but constrained by the technical installed capacity. Most HP is generated by impounding water behind dams (or weirs), which enables control of the amount of water driving the turbines and leads to an increased hydraulic head. Run-of-river hydropower plants just rely on uncontrolled streamflow and generally have a lower head. So-called pumped-storage hydropower plants, where water is pumped to a reservoir at a higher elevation and released later at times of higher electricity demand, consume more electricity than they produce.

Both hydraulic head and water flows are temporally variable. In case of run-of-river HP, lower than normal streamflow, i.e. drought, immediately reduces water flow through the turbine and thus HP, while in case of reservoir-based HP, lower than normal streamflow flowing into the reservoirs may require a reduction of water flow through the turbines only later. Still, unless streamflow deficit is small compared with the storage capacity of the reservoir, HP is reduced during streamflow drought for both types of hydropower plants, negatively affecting both hydropower suppliers and consumers. In 2016, drought caused severe reductions in hydroelectricity supply with negative effects on daily life and the economy in Venezuela (Hambling, 2016). Two consecutive monsoon failures had reduced reservoir storage in India such that HP was significantly lower than normal in 2015–2016, with 15% less HP than the previous year in some plants, while electricity demand due to a heat wave (often concurrent to less precipitation than normal) was higher than normal (Singh & Sally, 2016). HP reduction due to drought is particularly problematic in countries that strongly rely on hydropower for their electricity supply, which include many countries in Africa and South America (EIA, 2019). For the western US states, it was found that droughts caused a shift in electricity production from fossil fuels, increasing air pollution (Herrera-Estrada et al., 2018).

There are a number of continental- or global-scale studies about the impact of climate change on the potential for HP (Herrera-Estrada et al., 2018; Van Vliet et al., 2016a; b). Impact of drought on HP was only investigated for small regions and some countries such as Finland (Jääskeläinen et al., 2018) and Canada (Bonsal et al., 2011), and in one global study of Van Vliet et al. (2016c), HP reduction in selected drought years was quantified.

Operational drought monitoring systems that aim to inform about current drought conditions, such as United States Drought Monitor (USDM, https://droughtmonitor.unl.edu/), the South Asia Drought Monitoring system (SADMS, http://dms.iwmi.org/), and the European Drought Observatory (EDO, https://edo.jrc.ec.europa.eu/), generally include on indicators of the physical drought hazard, i.e. indicators that quantify the degree to which there is less water than normal, e.g. less precipitation or less soil moisture than normal. Impacts of drought, which derive from the combination of hazard, exposure and vulnerability (IPCC, 2014) are not included, except the remote sensing-based NDVI, a measure of vegetation health. Global drought impact analyses found in the literature focus on impacts on agriculture (IPCC, 2014) or try to quantify a broad overall impact for countries with their agriculture and water supply sectors (Carrao et al., 2016).

In this study, we assess the impact of drought on HP at the global scale and propose indices that inform about HP risks, can be computed with the developed HP model in near-real time and may therefore be included in a global drought monitoring and early warning system. First, we compiled a new comprehensive global hydropower database (GHD) and HP model that is suitable for computing HP at the global scale. In section 3, HP anomalies due to streamflow drought are presented and then ways of providing HP information in a drought monitoring system are explored. Section 4 briefly discusses limitations of the HP model and finally conclusions are drawn in section 5.

2 Methods and Data

The amount of hydropower electricity HP_t [kWh] produced over a time period Δt can be quantified as using the following equation (El-Hawary & Christensen, 1979; Wan et al., 2020; Zhao et al., 2014)

$$HP_t = \min(\eta Q_{t,turb} H_t, N_{installed}) \cdot \Delta t \qquad (1)$$

where η is a comprehensive hydropower efficiency [kW/m^4 s^{-1}] that combines acceleration of the earth, density of water and an efficiency term, $Q_{t,turb}$ is rate of water flow through the pipes and turbines [m^3/s], H_t is hydraulic head with respect to the outlet of the pipes [m], i.e. the difference between elevations of forebay and tailwater, and $N_{installed}$ is the installed capacity of the hydropower plant [kW], i.e. the maximum power output that can be produced by a specific plant. To enable the application of Equation 1 for simulating HP globally from 1975 onward, the location, type and installed capacity of ideally all but at least a large part of all hydropower plants (or of the globally installed capacity). H_t and $Q_{t,turb}$ must be estimated for all hydropower plants and time steps. As daily values of streamflow that are simulated by global-scale hydrological model are much less reliable than monthly values, HP is simulated with a monthly time step based on monthly streamflow values of the global hydrological model WaterGAP. The spatial resolution is the spatial resolution of WaterGAP, 0.5° longitude by 0.5° latitude (55 km by 55 km at the equator). WaterGAP streamflow values can be assumed to represent $Q_{t,turb}$ of the hydropower station within the grid cell as WaterGAP also simulate the water balance of large reservoirs. H_t of all considered hydropower plants is derived from databases, topographic data and WaterGAP simulation of water storage in reservoirs. Thus, HP model presented and applied in this study relies on two main input, the newly developed global hydropower database GHD (section 2.1) and output of WaterGAP (section 2.2). The HP model is introduced in section 2.3

2.1. A New Global Hydropower Database

Despite the recognition of environmentally sustainable hydropower to modern society, the reliable and open-access global databases describing the geographical distributions and characteristics of hydropower-plants are still largely incomplete. To address this shortcoming, an effort is initiated to collate currently developed/under-construction hydropower plants: the global hydropower database (GHD). We exclude the future changes in plants' distributions and installed capacities.

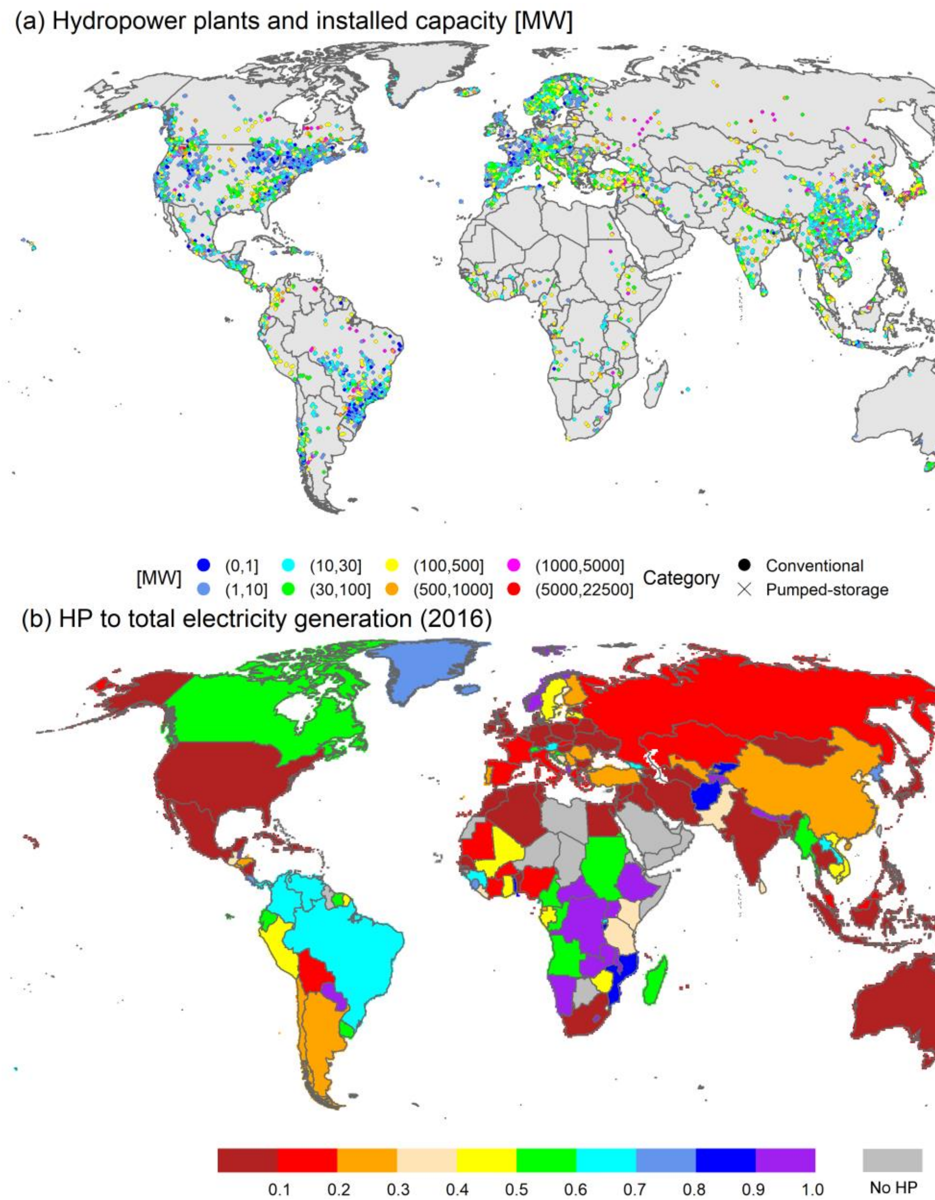

Figure 1. Installed capacity and plant category of the hydropower plants included in GHD (a), and the conventional HP as a fraction of total electricity generation $r(HP)$ in countries in 2016 according to EIA statistics (2019) (b). Conventional plants include both reservoir-storage and run-of-river plants.

The GHD contains 8748 records of hydropower plants distributed across 134 countries worldwide, including 87.4% reservoir-storage plants, 9.3% run-of-river plants and 3.3% pumped-storage plants. The GHD comprises only hydropower plants with installed capacities above 1 MW or plants where the associate reservoir has a storage capacity above 0.1 km^3. The spatial distribution and installed capacities of the hydropower plants included in GHD are shown in Figure 1a. The total installed capacity of all hydropower plants commissioned before 2016 is 1.147 TW, contributing 91.84% of the documented data of EIA (2019). 76.0% of total installed capacity is related to reservoir-storage hydropower, 10.3% is run-of-river hydropower and 13.7% is pumped-storage hydropower. In some countries, HP accounts for more than 90% of total electricity production in 2016, while only a few countries do not harness hydropower at all (Figure 1b).

The GHD leverages a wide variety of sources. Most information was taken and merged from the freely available databases World Power Plants Database (WPPD) (Global Energy Observatory, 2016), Global Power Plant Database (GPPD) (World Resources Institute, 2018), and Global Reservoir and Dam Database (GRanD) version 2019 (Lehner et al., 2011) (compare Table S1). We also included plants that are not listed in these databases from scattered data sources, such as HTML sources (e.g. Wikipedia), AQUASTAT (http://www.fao.org/aquastat/en/), CDM (https://cdm.unfccc.int/about/index.html) or research articles (see section S1 for more details). In addition to the compilation of data from these sources, GHD also contains derived estimated values as not all data required to implement Equation 1 were available from the data sources. GHD contains 43 attributes per hydropower plant. Table 1 provides an overview of key attributes in GHD, while a complete attribute list is found in Table S2.

Table 1. Overview of the content of GHD, providing the number of hydropower stations for which key attributes were available, the percentage of global installed capacity covered and the sources of the data. Details on data sources are provided in section S1 and Table S1. A complete list of attributes is provided in Table S2.

Key attributes/Description	Number of hydropower plants	$N_{installed}$ covered	Sources
Plant name, geo-location, nominated and actual installed capacities	8748	100.0%	Various sources, regression model for 500 stations
Maximum hydraulic head (H_{max})	871	29.7%	Wikipedia, CDM
Dam/weir height (H_{dam})	4169	75.8%	GRanD, other
Commissioning year (first year plant generated electricity)	5391	90%	GPPD, other
Dividing opening years with specific operational status (short operation, recommission, damaged, refurbish, unfinished)	84	6.6%	other
Started operation after 2016	41	3.9%	other
Annual HP estimation	7004	83.5%	GPPD, Wikipedia
Reservoir storage capacities, surface area, mean streamflow, upstream catchment area	2524	54.4%	GRanD, other
Reservoir operation is explicitly simulated in WaterGAP	705	28.2%	GRanD, WaterGAP

Each hydropower plant and, if any, associated reservoir was allocated to the appropriate 0.5°×0.5° (around 55 km×55 km at the equator) grid cell. This cannot be done by just taking into account latitude and longitude information of the plants but each plant has to be co-registered in accordance to the river network used in WaterGAP, the 0.5° global drainage direction map DDM30 (Döll & Lehner, 2002). Specially, all plants were situated along the DDM30 river network or at the adjacent cells near the river network, which required intensive manual checking. For some plants with more specific flow-accumulation information, additional tedious adjustments to the plant geographical location were also implemented to ensure reasonable consistency (1) the upstream catchment area defined by the DDM30 and those collected (partly) in GHD should be consistent or close; (2) compare the reservoir storage capacities of plants in GHD with GRanD reservoirs, i.e. the such plants should be located in the outflow cells of GRanD reservoirs. Therefore, geo-locations and up- and downstream topologies of some plants may be modified a bit as compared with their original sources.

The allocation of plants allowed for the linkage between GHD and WaterGAP that is necessary to compute HP according to Equation 1. In GHD, WaterGAP-derived attributes like catchment area, routing area, basin ID, the simulated long-term mean highest and lowest monthly streamflow at all plant sites, and the simulated mean reservoir storage for 705 plant sites are included. Also included in GHD is the gridded elevation difference (H_{ele}) between the cell where the hydropower plant is located and the downstream cell as this parameter was needed to estimate H_t (Equation 1 and section 2.3.1) for many hydropower plants. The H_{ele} was computed based on HydroSHEDS, a 30-arc-second global digital elevation map (Lehner et al., 2006) distinguishing cells with flow direction to its lower neighbor (i.e. cross-flow cells) from those at the lowest point of each pit (i.e. internal-flow cells). The elevation difference of the cross-flow cell was calculated by assuming streamflow falls from the mean elevation of the considered cell to that of the lower neighboring cell (i.e. $H_{ele} = \Delta L_{mean}$). In contrast, the streamflow for the internal-flow cell is assumed, on average, falls from the mean elevation to the minimum elevation per cell; the elevation difference was then derived as the difference between the two elevations of the internal-flow cell (i.e. $H_{ele} = L_{mean} - L_{min}$).

2.2. WaterGAP

WaterGAP 2.2d (Müller Schmied et al., 2014) is a 0.5° grid-based global-scale hydrological model that simulates both human water use as well as freshwater fluxes and water storages on all continents of the Earth except Antarctica with a daily time step. Differentiating surface water bodies and groundwater as sources and sinks of water withdrawals, it estimates water withdrawal and consumption for five sectors: irrigation, livestock farming, domestic use, manufacturing water use, and thermal power plant cooling (Döll et al., 2014). Based on the simulated time series of net groundwater, time series of climate data and many physiographical data, daily water balances of up to 10 storage compartments are computed for each of the 67,420 grid cells. For this study, the global daily WFDEI-GPCC dataset (Müller Schmied et al., 2016) was used as climate input. Runoff from land is routed through groundwater and surface water bodies (i.e. lakes, man-made reservoirs, wetlands, and rivers) storages along the drainage direction. WaterGAP simulates water storage dynamics of and outflow from the 1109 largest reservoirs worldwide (storage capacity $\geq$0.5 km^3) and 52 regulated lakes (area $\geq$100 km^2) based on the GRanD database version 1.1 (Lehner et al., 2011; Müller Schmied et al., 2014). 705 of the 1161 large-reservoirs/regulated lakes have HP as either the most important or the second most important purpose. Simulation of reservoir operation in WaterGAP distinguishes reservoirs with the main purpose irrigation from all others (Döll et al., 2009). Different from other global hydrological models, WaterGAP is calibrated against observed long-term average annual streamflow at 1309 gauging stations, with the purpose of obtaining meaningful estimates of water resources despite a number of sources for significant uncertainty in global hydrological modeling (Müller Schmied et al., 2014). This is one of the reasons why WaterGAP has been shown to provide better fits to streamflow observations than most other global hydrological models (Zaherpour et al., 2018).

WaterGAP output used for the HP include streamflow time series of streamflow (impacted by human water use and man-made reservoirs) Q_t for each grid cell as well as well as time series of the outflow $Q_{t,out}$ and water storage S_t of the 705 large reservoirs with the purpose of HP for the period 1975–2016. Monthly time series aggregated from daily values served as input for the HP model.

2.3. HP Model

The developed HP model takes into account only conventional hydropower plants, i.e. reservoir-storage and run-of-river plants. The electricity produced by the pumped-storage plants in GHD is not included in this study because (1) pumped-storage plants do not produce net electricity but as serve as energy storages (House et al., 2018), and (2) data for calculating pumped-storage HP such as operating period, pumping rate as well as lift and drop heights are lacking (Schill & Kemfert, 2011).

The HP model simulates monthly time series of HP for each conventional hydropower plant in GHD based on Equation 1. Figure 2 provides the flowchart of plant-specific HP. To implement Equation 1, the comprehensive hydropower efficiency η, which usually ranges from 6.5 to 8.5 kW/m^4 s^{-1} depending on water conduit and turbine types (Bakis, 2007; Zhou, 1997), is set to 8.5 kW/m^4 s^{-1} for large hydropower plants with an installed capacity $N_{installed}$ of more than 30 MW (Department of Energy, 2019) and to 8.0 for kW/m^4 s^{-1} smaller plants. The time step interval Δt is set to 1 month assuming non-stop HP. Turbine release $Q_{t,turb}$ is specified for two cases. For the 705 large reservoir plants whose reservoir operation processes are explicitly simulated in WaterGAP 2.2d, we assume that all reservoir outflow goes through the turbines unless installed capacity is exceeded, i.e. $Q_{t,turb} = Q_{t,out}$. For all other plants, the turbine release is assumed to be equal to WaterGAP 2.2d gridded streamflow time series, i.e. $Q_{t,turb} = Q_t$.

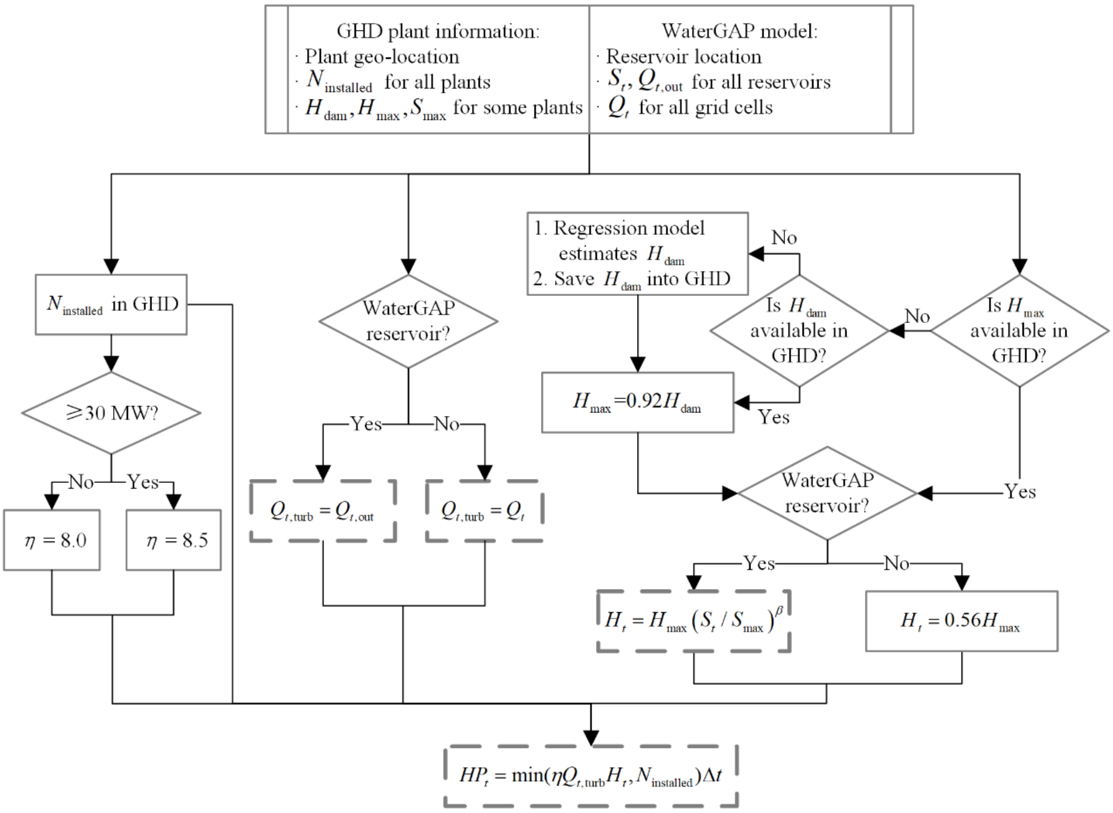

Figure 2. HP simulation process using GHD and WaterGAP data as input. Boxes with solid lines indicate temporally constant variables, those with dashed lines indicate monthly time series.

Estimation of hydraulic head H_t also differs between the two plant groups but does not distinguish run-of-river plants from those reservoir-storage plants that are not among the 705 plants for which WaterGAP explicitly simulates reservoir storage. H_t is determined in two steps (Figure 2). In step 1, maximum hydraulic head H_{max} is set and in step 2 H_t. If H_{max} is available for a plant in GHD, we used this value directly. Otherwise, if H_{dam} is available,

$$H_{max} = 0.92H_{dam} \tag{2}$$

Dam freeboard (the safety margin for maximum water storage in the reservoir) is usually 4% – 5% of dam height (Ali et al., 2012) and an equally tailrace water height was assumed. If there is neither a H_{max} nor a H_{dam} record, a multiple linear regression model was set up to estimate H_{dam} from GHD attributes of installed capacity of plant, gridded elevation difference and long-term mean highest and lowest monthly streamflow at plant sites. Visual inspection revealed no evidence of multicollinearity among these predictors. The regression model was first fitted for the 4111 plants with reliable observation of dam/weir height in GHD (correlation coefficient of this model R = 0.5 after removing outliers with studentized residuals that were larger than 3 in absolute value), and then used to assess the dam height for the remaining plants. Due to the poor correlation, minimum simulated dam height is set to 2 m, and for plants with installed capacity lower than 100 MW, H_{dam} was not allowed to exceed 200 m. The values of three predictors and estimated H_{dam} are all listed in GHD.

In case of the 705 large reservoir hydropower plants, H_t is assumed to vary from month to month as a function of reservoir storage, with

$$H_t = H_{max}\left(\frac{S_t}{S_{max}}\right)^{\beta} \tag{3}$$

where S_t is WaterGAP 2.2d simulated monthly reservoir storage [m^3], S_{max} is the maximum reservoir storage (listed in GHD) [m^3] and β =0.9229 is a regression parameter that relates storage variations to head variations and is taken from the GRanD technical document (Beames et al., 2019). For plants with smaller reservoirs or run-of-river plants, H_t is assumed to be temporally constant, with

$$H_t = \gamma H_{max} \tag{4}$$

where $\gamma = 0.64$ is a globally homogeneous calibrated parameter such that the simulated global gross HP in 2016 is proportional to the EIA statistic, taking into consideration of installed capacity coverage included in GHD.

For any single power plant, the actual time series of electricity generation is linked to plants' operation status. When a plant is reported to be first commissioned/opened from a specific year (i.e. attribute Year_Open in Table S2), we then started to estimate the HP at the plant level. If this attribute is missing, we assume that this plant has already been commissioned before year 1975, which is the starting point of our simulation period. The operation status of plant can vary by time period due to maintenance, decommission, and accidental destruction (i.e. attribute Timeline in Table S2), we excluded the electricity generation during these non-working periods. The HP from plants that were still under refurbishment in 2016 or have been decommissioned/shut-down before 2016 were also excluded. Therefore, the monthly HP to the plant level that were operational during the time period 1975–2016 is determined.

Changes in HP are mainly due to commissioning and decommissioning of hydropower plants and streamflow variability, and HP data, e.g. annual HP country values from EIA, reflect both influences. To test the ability of the HP model to represent the impact of streamflow variability on HP, which is key for estimating the impact of drought on HP, three model variants of model output V0, V1 and V2 were simulated for the period 1975 to 2016: V0 takes into account the annually changing number of actually operating plants and the historical time series of hydrological inputs (i.e. Q_t, $Q_{t,out}$ and S_t). For V1, the historical hydrological inputs are applied for the hydropower plants existing in 2016, while in V2, 1975−2016 mean streamflow values per calendar month are applied for the annually changing number of hydropower plants of V0. Annual HP time series from all the three variants were used in a comparison to annual time series of EIA.

2.4. Quantifying Streamflow Drought Hazard

2.4.1. Indicator of Streamflow Drought Hazard

To quantify streamflow drought hazard, we use the standardized streamflow index (SSI, Vicente-Serrano et al., 2011). The SSI of an individual month can be interpreted as the number of standard deviations that streamflow in this month deviates from the mean streamflow of the calendar month. Both mean and standard deviations for the 12 calendar months are computed over a reference period, here 1975−2016. In this study, we selected a three-month accumulation period and analyzed SSI3 to focus the analysis on longer streamflow deficits and make model uncertainties, in particular regarding the operation of reservoir that may lead to seasonal shift less impacting. To compute SSI3 for each month and 0.5° grid cell during 1975−2016, monthly WaterGAP 2.2d streamflow was first averaged over the last 3 months for each grid cell. Then, these 42 streamflow values (1975−2016) for each calendar month were fitted to a Pearson type III distribution (see section S2 for the probability distribution tests) and finally transformed to a normal distribution via the associated cumulative probability, resulting the SSI3. The SSI3 of –1 indicates the streamflow averaged over the last three months was one standard deviation lower than the normal for the respective three calendar months.

2.4.2. Three-Dimensional Streamflow Drought Event Identification

As droughts are regional phenomena, it is of interest to quantify drought hazard not only for individual 0.5° grid cell, but to also identify large, spatially and temporally contiguous drought patches/events, and characterize them by their spatial extent, duration, severity and intensity (Andreadis et al., 2005; Dracup et al., 1980). Using the approach proposed by Haslinger and Blöschl (2017), we performed the following four main steps.

(1) Identify the grid cells that are "under drought". Following Agnew (2000), a drought is assumed to occur if SSI3 is less −0.84, which occurs on average once every 5 years (corresponding to an annual probability of non-exceedance F of 0.2). Each F of each SSI3 value < −0.84 is than mapped to the interval [0,1], with

$$q_{int,t} = \frac{0.2 - F(SSI3_t)}{0.2} \tag{5}$$

where F is the non-exceedance probability of SSI3 in period t. All grid points with positive $q_{int,t}$ for at least two consecutive months are considered as "under drought".

(2) Detect the spatial extent of drought. The 0.5° cells under drought are aggregated into different drought patches by searching their 3×3 neighborhood grids. Once a continuous drought area exceeds a threshold of 25,000 km^2 (around 9 grid

cells in the equatorial regions), it is considered as a drought event with reasonable size and therefore impact (Liu et al., 2019). With this approach, smaller drought patches are filtered out. In our study, only 13% of all grid cells and months, for which a positive $q_{int,t}$ was determined throughout the study period, were identified to belong to such reasonable large drought patches.

(3) Determine the temporal connection between drought patches. Because one single drought event in a month can break up into multiple smaller drought events, or several small droughts merge into one spatially larger event in the subsequent month, we assume that the drought patches in two consecutive months belong to one drought event if drought area overlap is larger than 50% of the area of the smaller patch while the denominator itself is no less than one quarter of the area of the larger patch.

(4) Extract drought features. The drought event duration is defined as the months between earliest initial and latest terminal time of all related grid points in the same event. For every time step, the monthly intensity is measured as sum of the gridded $q_{int,t}$ of the current drought patch. And the drought severity is the cumulative monthly intensity over the whole drought duration.

2.5. Estimation of Probability of Exceedance of HP Reduction for Risk Analysis

HP deficit is computed from HP computed with model variant V1, i.e. with historical streamflow time series and hydropower plants that existed in 2016. For the same reasons as for aggregating streamflow over three months (section 2.5.1), we averaged also HP, for each month between in the period 1975−2016, over the last three months to obtain HP3. For a specific hydropower plant, HP deficit Def_t occurs in months where HP3 is less than the long-term mean over the same months ($\overline{HP3}$) for each plant.

$$Def_t = \begin{cases} \overline{HP3_t} - HP3_t & if\ HP3_t < \overline{HP3_t} \\ 0 & others \end{cases} \tag{6}$$

For analyses at the grid cell level and country level, HP3 of each plant within a grid cell or a country was first added up to the grid/national total HP3 before calculating indicators as above. This manipulation is reasonable because HP produced by individual hydropower plant is distributed via regional power transmission networks, such that the HP deficit has only limited impact. HP deficit events may last for a few months to multiple years. Severity of each identified HP deficit event $Sev(HP)_i$ is calculated as the sum of the monthly deficits over the event duration as

$$Sev(HP)_i = \sum_{t=s_i}^{l_i} Def_t \tag{7}$$

where s_i and l_i are the first and last time steps of an HP deficit event *i*. It quantifies the amount of hydroelectricity that could not be produced due to dryer than normal conditions.

Each HP deficit event can be described by the probability that its severity is exceeded, applying the threshold method used for flood frequency analysis (Smith, 1984). The severities of all identified HP deficit events are ranked based on their magnitudes. Then, a Pareto type II distribution was fitted to the top 42 HP severity values in the 42 years of 1975–2016 to estimate the probability that in any year a HP deficit event occurs that does not exceed the severity of interest (see section S2 for the distribution tests). If there were less than 42 historical deficit events, the remaining events are fill by 0, representing ignorable severity of HP deficit. HP reduction during one event is expressed in terms of mean annual HP by dividing severity by mean annual HP.

3 Results

3.1. Performance of GHD and HP Model

Performance of WaterGAP streamflow has already been extensively tested(e.g. Müller Schmied et al., 2014; Zaherpour et al., 2018). Therefore, we focus here on the validation of GHD (section 2.1) and HP simulations of model variant V0 (section 2.3/2.4) mainly using the statistics-based country-level data from EIA (2019). Figure 3 compares the total installed capacity from EIA and GHD in 2016 at the country level, for 134 countries. The six world regions are divided according to the International Hydropower Association (IHA) regional classification (IHA, 2018). For 94.8% (i.e. 127) of the 134 countries, the differences in conventional installed capacities between EIA and GHD are within 10% or 0.1 GW. The largest absolute discrepancy is found for China, were GHD misses 23.6% of the EIA installed capacity (Figure 3a, highest value show refers to China). Countries with relative discrepancy higher than 50% are found equipped with EIA installed capacities less than 0.2 GW. Figure 3a also reveals that most countries in Africa hold conventional installed capacities of up to only 1.0 GW, while the opposite is true in the other five regions. The ten counties with the top conventional installed capacities are, in descending order, China, Brazil, Canada, United States, Russia, India, Norway, Turkey, Japan and France. Although this study does not consider the power production generated by pumped-storage plants, the GHD compiles 285 records for pumped-storage relevant data. Merely 41 out of 134 countries have pumped-storage plants and the largest two countries are in East Asia, i.e. China (29 GW) and Japan (27 GW) (Figure 3b). On average, the linear relationship indicates a good hydropower plant coverage by GHD, indicating the reliability of the GHD in terms of installed capacities and spatial distribution and its suitability for studying HP at the global scale.

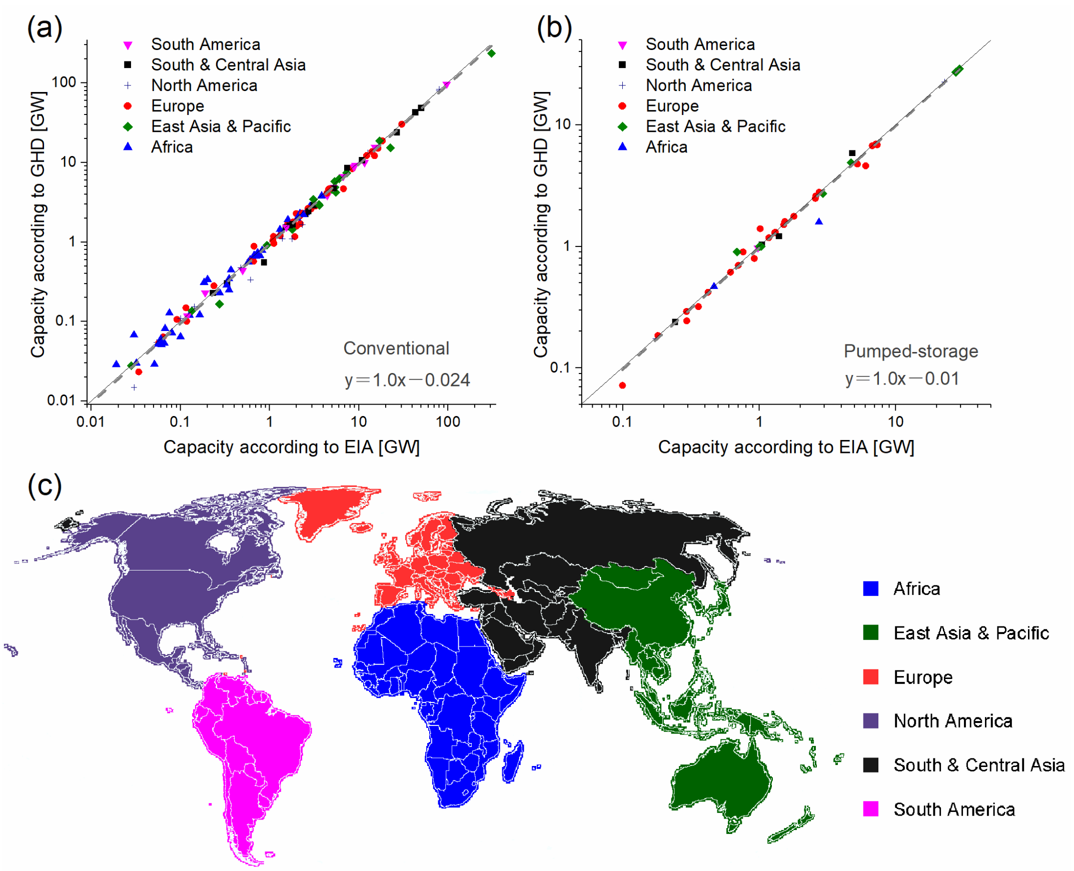

Figure 3. Comparison of country-level total installed hydropower capacity between EIA (International Energy Statistics) statistics and GHD for the year 2016 distinguishing conventional (reservoir-storage and run-of-river) plants (a) and pumped-storage plants (b). The countries are categorized into six world regions

according to IHA(2018)(c). The solid lines in (a) and (b) represent 1:1 relationship, and dashed ones are the linear regression curves (R^2 =0.99 in both cases).

To test the capability of the HP model of simulating drought impact on hydroelectricity production, one would ideally compare simulation results to, e.g. monthly statistics of HP of individual plants. As an example, Figure 4 shows the time series of simulated monthly HP for the United States as compared with the EIA statistics (2019). A good fit of HP simulation to statistical HP time series is obtained. The seasonal and annual variabilities are captured well. In general, low values of HP are represented very well by the HP model, which is shown by very good correspondence between simulated and statistical monthly minimum (Figure 4). The high values of HP are somewhat overestimated, thereby resulting a relative low overall Nash-Sutcliffe efficiency (NSE=0.31). This might be due to the issue of overcapacity in hydropower generation in high flow seasons, when electricity generated from other sources are sufficient to meet all the demand.

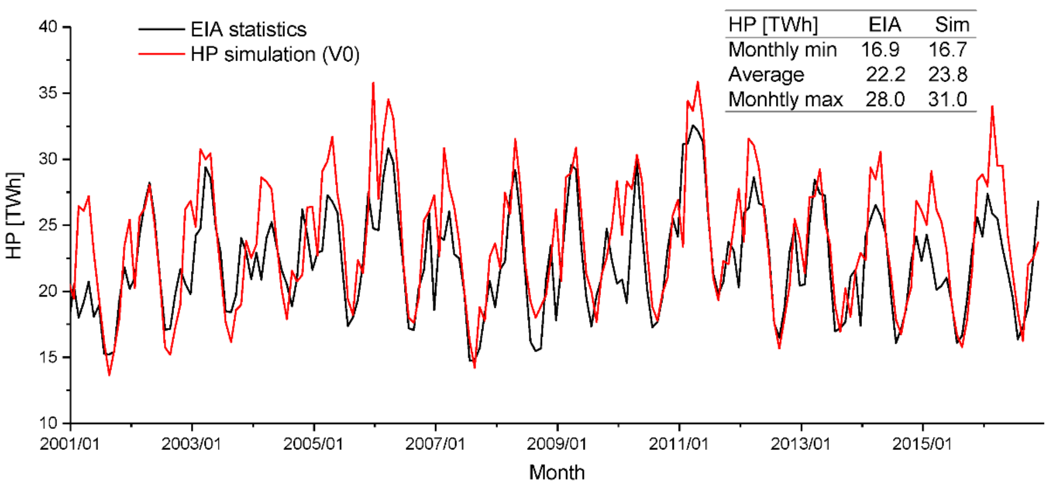

Figure 4. Monthly net generation of conventional hydroelectric [TWh] for the United States from 2001−2016: comparison between EIA statistics and HP simulation of

model variant V0.

For a global-scale validation of the HP model, only annual time series of HP per country were available starting from 1980. NSE, coefficients of variations and the ratio of simulated over observed coefficient of variations vary strongly among countries (Figure S1), with best values for China, India, Mexico, Mongolia, South Korea, Spain and the United States, and worst values in Africa but also Australia. The bad performance in Africa countries is mainly due to the sparse hydropower plants and small quantities of total installed capacities; therefore, even minor inconsistency in plants can result in apparent HP deviation from the statistics. For many countries, the annual time series are dominated by a strong upward trend due to an increasing number of hydropower stations, not by climatic variations (e.g. China, Figure S2). Figure 5 presents a comparison of simulated and observed annual time series of HP (V0) for all power plants within the six world regions for 1980−2016. The HP trends in the world regions are well captured by the HP simulation, except for the East Asia & Pacific regions. The latter is due to the incomplete records on installation of new hydropower plant, particularly in China, which contributes most to the overall rapid increase behavior of regional HP (Figure S2). The observed interannual variabilities in North America and Europe are simulated well by the HP model (Figure 5). In case of Africa, however, statistics do not support the international variations around the trends that is simulated. In the other three world regions, the annual time series are dominated by trends.

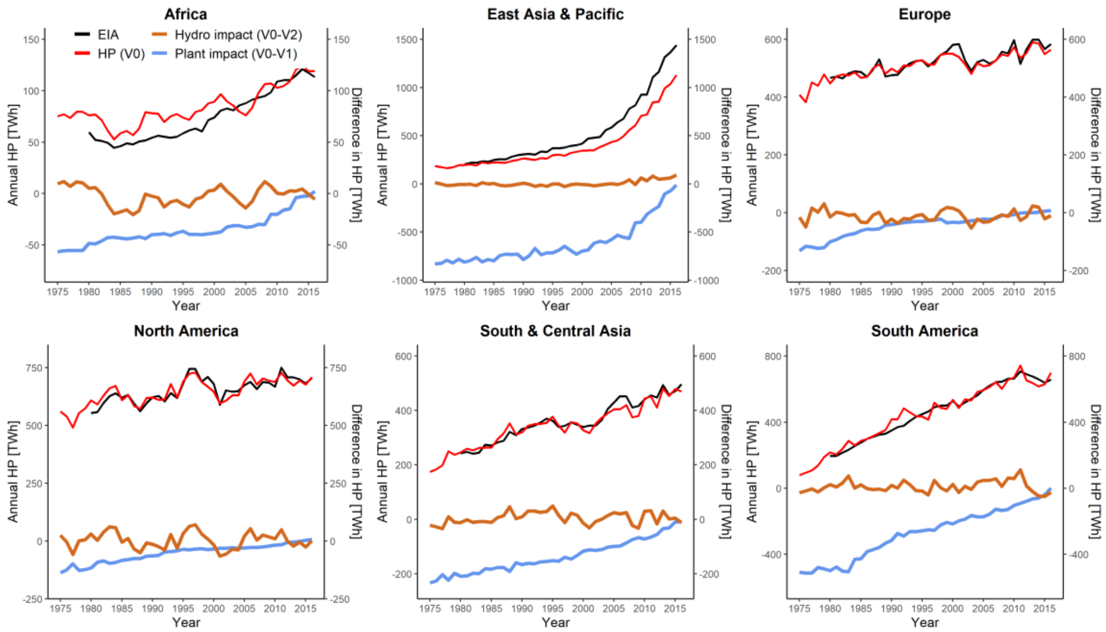

Figure 5. Series of long-term annual HP and HP differences for the six world regions during 1975–2016. Red lines show the simulated HP (V0), black lines EIA statistics (1980–2016). The brown line represents the impact of hydrological variability (difference between V0 and V2, simulated by assuming mean monthly streamflow) on simulated HP, the blue line the impact of plant variability (difference between V0 and V1, simulated by assuming a constant number of plants).

Figure 5 also shows the results of decomposing the HP time series obtained considering climate variability and the changing number of hydropower plants (V0) into the impact of hydrological variability (brown lines) and of plant variability (blue lines). The positive trend of plant-impact lines in all six regions are due to increasing values of total installed capacities. The occasional fluctuations suggest the unexpected shutdown or decommissioning of some large plants in those specific years. The hydro-impact lines do not show any significant trends but large variations around the zero mean, with negative values (of differences between the HP simulation with actual streamflow and the simulation with long-term mean monthly streamflow) indicating unusually dry years. For example, Africa witness three obvious valleys in 1982–1988 and 2002–2006, which coincide with reported extreme droughts in Africa (Masih et al., 2014). Equally, large North America drought around 1977, 1988 and 2002 (Andreadis et al., 2005) are represented in the HP simulation.

3.2. Drought Impact on HP

3.2.1. Performance of Streamflow Drought Simulation

Simulation of HP drought impact relies on a reliable simulation of streamflow and in particular streamflow drought. Therefore, we tested the performance of simulated monthly streamflow and drought indicator (SSI3) against observations at 183 stations (Figure S4) worldwide for which continuous time series of monthly streamflow are available during 1971−2000 (more details are provided in section S4). The observed streamflow was provided by Global Data Runoff Centre (GRDC). The agreement of NSE for SSI3 was moderate with a median of 0.5 and an interquartile range between 0.2 and 0.7 (Figure S5). The goodness-of-fit for streamflow is very similar, albeit with slightly lower quartile of 0.14. At 25 stations (41% of assessed basin area), both NSEs exceeded 0.7. At a large number of stations (83% of assessed basin area), simulated and observed SSI3 values were classified into the same drought hazard class in 70% of the time (Figure S6).

3.2.2. HP Reduction during Large Contiguous Droughts

Globally, a total of 14,641 large contiguous drought events are identified in the period 1975 to 2016 according to the method explained in section 2.4. During these

42 years, several prolonged as well as widespread droughts have occurred. Table 2 summarizes the drought characteristics of the 20 most notable events in terms of severity, which are in agreement with the major drought events reported in the literature (Bonsal et al., 2011; Masih et al., 2014; Spinoni et al., 2015; Zhang & Zhou, 2015). From the listed events, areas of Northern Europe (and Russia) and Northern America show the highest drought frequency and severity between the 1970s to 2010s, making up 13 of the top 20 events.

Table 2. Twenty most severe streamflow drought events affecting a large contiguous region over a long time period, ranked by severity according to the definition described in section 2.4. A severity of 5000 could be due to, e.g., the existence of a drought patch with on average 1000 cells with a 1-in-10 year drought occurrence ($q_{int,t}$= 0.5) over on average 10 months. HP reduction (V1) indicates the relative deviation from the mean monthly HP (V1, based on 2016 hydropower plants) over 1975–2016. $N_{installed}$ coverage refers to, during a drought event, the maximum percentage ratio of the affected total installed capacity of all hydropower plants (incl. pumped-storage) that are included in GHD and have been in operation before 2016.

Rank	Affected region	Period	Duration [month]	Severity	HP reduction (V1)	$N_{installed}$ coverage
1	Europe	04.1975-08.1977	29	41661	13.8%	15.9%
2	Central Russia	12.1984-03.1988	40	32887	28.3%	1.1%
3	Sahel region of Africa	07.1981-08.1987	74	30813	20.4%	1.2%
4	North American	12.1986-11.1992	72	23999	6.5%	11.1%
5	North American	10.1995-10.2001	73	21980	4.3%	7.6%
6	North American	05.1998-06.2003	62	21121	1.3%	5.7%
7	Central Russia	06.1981-08.1983	27	21116	19.5%	3.2%
8	Australia	07.1986-12.1991	66	18530	1.0%	0.1%
9	Northern Canada	07.1994-08.1998	50	18030	8.0%	0.1%
10	Northern Europe & Russia	01.1996-10.1997	22	16756	10.1%	11.3%
11	East Asia, mainly China	07.2002-04.2005	34	15807	4.4%	10.9%
12	Europe	02.2002-08.2005	43	15719	4.2%	14.7%

13	Africa	01.2009-10.2011	34	15175	8.0%	1.2%
14	South America	04.1997-10.1999	31	14544	4.1%	7.4%
15	North America	05.2003-03.2005	23	14337	9.9%	7.3%
16	South America	10.1991-02.1994	29	14198	4.9%	5.3%
17	Russia	07.2011-04.2013	22	13754	6.4%	1.0%
18	Europe	07.1983-04.1985	22	13120	9.4%	7.9%
19	United States	12.2010-02.2015	51	13036	7.4%	4.9%
20	South Asia	08.2000-11.2002	28	12578	15.0%	7.1%

Among these top events, the 1976 European drought that occurs between April 1975 and August 1977 is ranked as the most severe one, which lasts for 29 months and sweeps 5.9% of worldwide gross installed hydropower capacity in 1977. According to the 2016 hydropower plants level (model variant V1), this $N_{installed}$ coverage even reaches 15.9% and the simulated HP reduction is 13.8% (Table 2). Since 2000, Europe has witnessed a series of extreme dry events in combination with heatwaves, e.g., 2003, 2010 and 2015 (Laaha et al., 2017; Schewe et al., 2019). The detected 2003 European drought (ranked 12, Table 2) holds from February 2002 to August 2005, and reaches its peak in September 2003, with a total severity of 15719.

3.2.3. Analysis of HP Reduction during the 2003 Central European Drought

To reveal how streamflow drought influences HP at the country scale, we took the 2003 European drought, focusing on the central European countries (hereafter referred to as “2003 CEU drought”, Figure 6a). The 2003 CEU drought was classified as a 30-year drought, i.e. a drought with a return-period of 30 years, based on temperature data (Charpentier, 2011). The 2003 CEU drought began in early in early spring (February 2003) and intensified from June, then rapidly expanded to cover 75% area of Central Europe in August. The drought began to quickly recede in October and completely disappeared in March 2004 (Figure 6b). Drought duration was longest in Poland, where most grids were under drought for more than 7 months (Figure 6a). Northern Germany and eastern Hungary were least affected, with some grid cells without any negative streamflow anomalies.

Due to the low precipitation and extremely high temperature and thus low streamflow, the energy sector was challenged by a reduced potential of hydropower (Mukheibir, 2013). In CEU, most plants are concentrated in the south in Switzerland (CH), Austria (AT), Czech Republic (CZ) and Slovakia (SK) (Figure 6c). The time series of annual HP (V0) over CEU simulates well the strong interannual variability of HP shown by the EIA statistics, with years of high HP such as 1993 and 2013, and years of low HP reduction such as 1996, 1997 and 2010 being reproduced (Figure 6d). However, HP reduction in the drought year 2003 (but also 2015) is strongly overestimated by the HP model. Compared to 1980−2016, the simulated HP reduction is 11.4%, while according to EIA it is only 4.0%. Considering the CEU drought period February 2003 to March 2004, HP was reduced by 10.6% with respect to 1980−2016. The overestimation of drought impact in CEU during 2003 as compared with EIA statistics is due to an overestimation of HP reduction for two countries with the highest HP production, Switzerland and Germany (Figure 6e and Figure S3a, compare red triangles to blue circles for country-scale relative anomalies). In both countries, the statistical HP production was very close to normal. In Switzerland, runoff generated in high glacierized basins dominates the streamflow regime relevant for HP, with summer streamflow having increased over the last decades due to glacier mass loss (Hänggi & Weingartner, 2012). We assume that there are two reasons for the poor simulation of the 2003 drought impact on HP in Switzerland: (1) the lack of glacier mass balance modeling in WaterGAP; and (2) that the impact of electricity prices, which are known to have a significant positive effect on HP (Golombek et al., 2012), are not taken into account in the simulation of reservoir release. However, it is surprising that there was very little HP reduction in Germany according to EIA and a lot according to our model, as both the observed and simulated streamflow drought at two streamflow gauging stations on Danube and Rhine, which are downstream of the most important hydropower plants in Germany, are very strong (Figure S7). The simulated HP (V0) anomalies are quite consistent with the statistics in Austria (AT), the country with the third highest HP reduction, Czech Republic (CZ), Hungary (HU) and Slovakia (SK), and relatively close for Slovenia (SL). A previous evaluation of Schewe et al. (2019) claimed that their hydropower model constructed by Van Vliet et al. (2016b), using VIC global hydrological model, mostly tends to overestimate the hydropower impacts. Our HP results are similar to those findings.

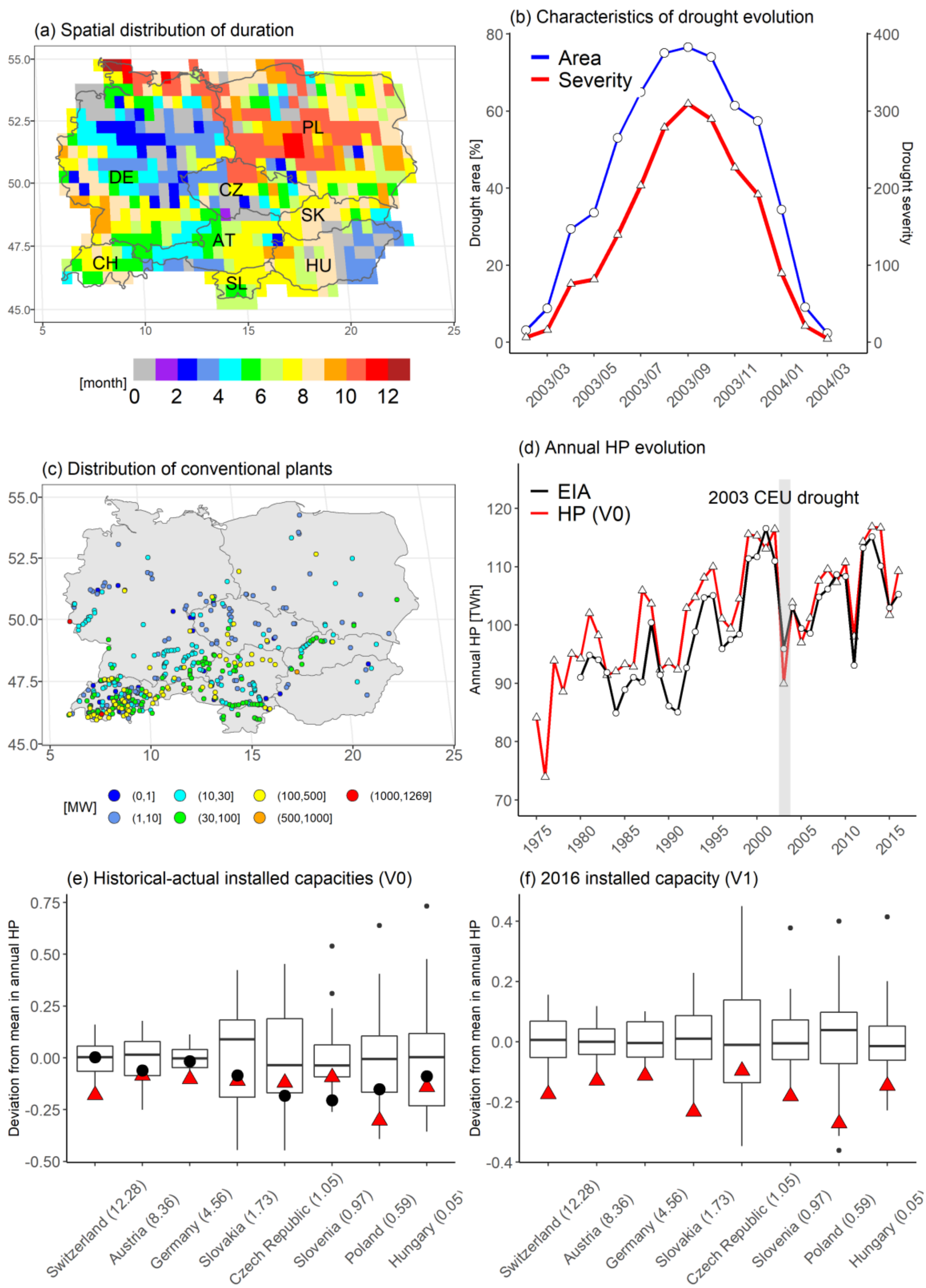

Figure 6. Spatial-temporal evolution of 2003 CEU streamflow drought in terms of drought duration in month (a), and total severity and areal coverage (% of CEU area) (b); spatial distribution of conventional hydropower plants with installed capacity (c), and historical annual total HP simulation (V0) in CEU as compared with EIA statistics

for 1980–2016; box-plot for HP (V0, based on time-varying hydropower plants) and HP (V1, based on 2016 hydropower plants) showing the simulated relative deviations from the long-term mean annual HP over 1980–2016 for all hydropower plants with the respective country as a whole (e, f). Countries are ordered by installed capacity in GW as included in (c). The filled red triangles in (e, f) are the simulated mean relative deviations in year 2003, and filled black circles in (e) are derived from EIA data.

To isolate the drought impact on HP reduction, HP during the drought period should not be compared with the time series of actual HP within any spatial unit as this includes the impact of the number of active plants on HP. Evaluation of the V1 runs, with a constant distribution of hydropower plants, results in larger reductions from normal conditions during 2003 (Figure 6f and Figure S3b). All counties, except Czech Republic, are simulated to suffer reductions of more than 15% reduction, or around 1.0–2.0σ.

3.3. Risk of HP Reduction due to Drought

Each plant, grid cell or other spatial units is under a certain risk of HP reduction due to drought, which can be expressed as the probability that a certain reduction in percent of the normal annual HP is exceeded with a certain probability in each year. We assume that probabilities of exceedance can be derived from historical HP time series as derived from historic streamflow time series. Then, using the method described in section 2.5 and constant (year 2016) hydropower plant distribution (HP V1), we computed, for 0.5° grid cells and whole countries, the percent HP reductions that can be expected to be exceeded with a probability of 0.1 in any year or, equivalently, in 1 out of 10 years (Figure 7). A value of 20% for example, in the maps means that during 1975−2016, there was a 10% change in any year that this location faced a reduction of at least 20% of its mean annual hydroelectricity production. Under non-stationary conditions, which are mainly due to climate change, these values in Figure 7 cannot be considered to be true probabilities and are only an approximation.

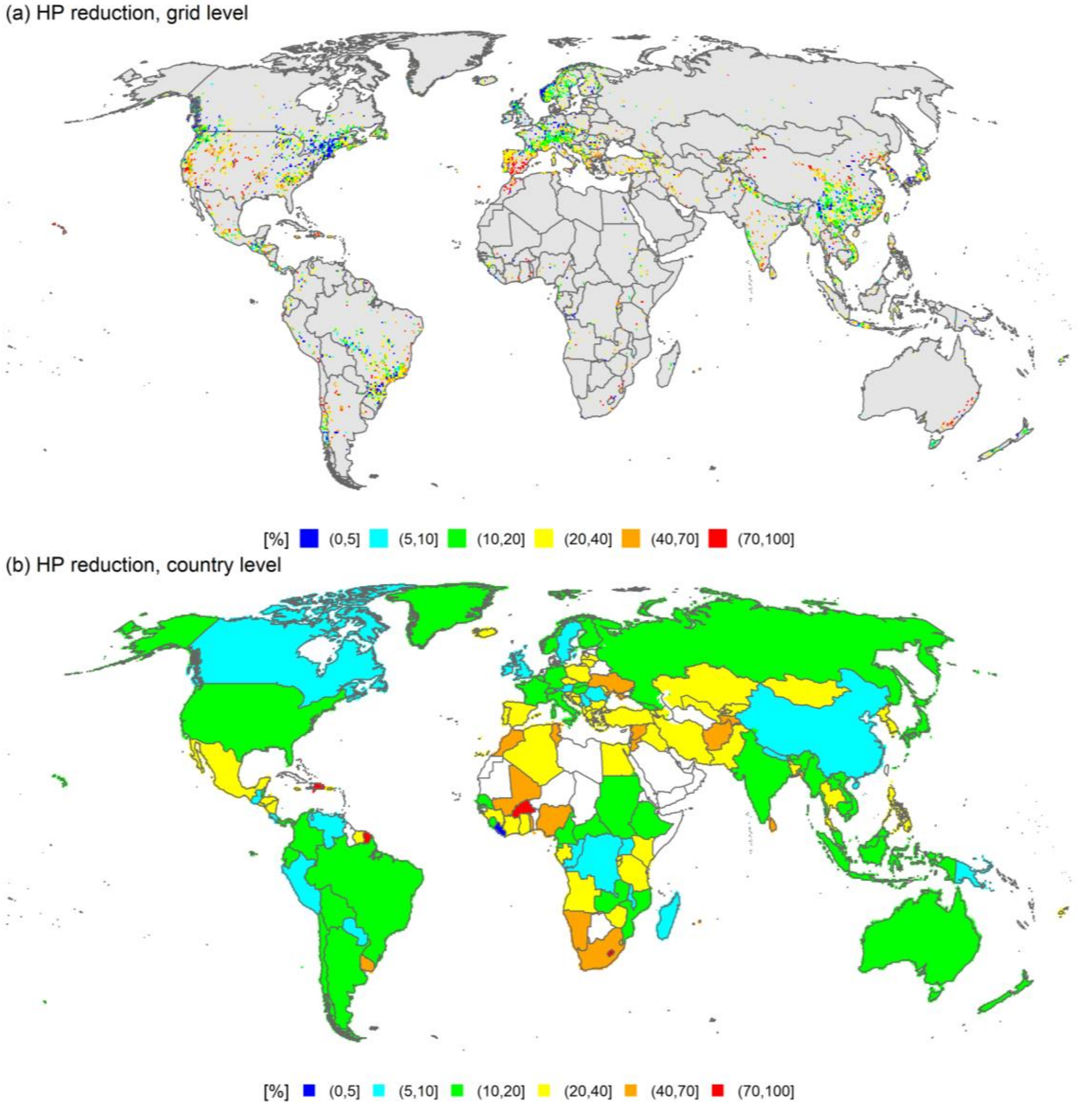

Figure 7. HP reduction in percent of mean annual HP that occurs in 1 out of every 10 years (i.e. with an annual probability of occurrence of 10%) at the grid level (a), and the country level (b), based on HP (V1) simulation for the period 1975–2016.

In 1 out of 10 years, 57% of all 4077 grid cells covered with power plants face a

HP reduction of more than 20%. HP reduction is particularly high in semi-arid areas, like western United States and the Mediterranean region, unless hydropower plants are located on large rivers. In 7% of the cells, HP is even expected to be reduced, in 1 out of 10 years, by more than 70% as compared with mean annual HP. In contrast, there is almost no HP reduction in 16% of the cells (HP reduction≤5%) when a 10-year HP deficit event occurs.

At the country level, HP reduction in 1 out of 10 years is between 4.4% in Liberia and 93.2% in Lesotho (Figure 7b). China, accounting of 21.5% of global HP, shows a very small HP reduction of only 7.5% even though many individual power plants are simulated to suffer from reduction of more than 10% or even 40% (Figure 7a). This is because (1) as a large country, if one region of the country suffers from a drought the other would not and vice versa; (2) most of the large Chinese hydropower plants are subject to very low reductions of less than 5%. A small value of reduction in China could be caused by such balancing. There are 63 out of 134 countries with relatively small HP reductions (≤20%), while 50 countries show moderate HP reductions between 20%–40%, including countries in Central America and the Middle East.. It appears that the majority of these moderately affected regions also have relatively low proportion of hydropower in energy (r(HP)≤0.3, Figure 1b). Countries with high HP reduction (>40%) are mostly found in Africa. Only four countries show more than 70% HP reduction, Dominican Republic, French Guiana, Burkina Faso and Lesotho. As hydropower is the only source of electricity production in Lesotho (i.e.

r(HP) = 1), our simulation results suggest that, in 1 out of 10 years, total electricity production in Lesotho is reduced to less than 10% of its long-term average.

3.4. Experimental Near-real-time Monitoring of Potential Drought Impact on HP

This section explores a set of monitoring indices that are suitable for informing about visualizing HP reduction in a global drought monitoring system.

3.4.1. Identifying Suitable Indicators for Monitoring

As a component of a drought monitoring and early warning system, HP indicators are to inform about the status of current HP as compared with HP occurring under normal streamflow conditions, in order to enable e.g., adaptive measures in case a certain reduction threshold is exceeded. For a holistic HP drought monitoring, we propose multiple indicators that quantify the amount and uncommonness of HP reduction at the scale of 0.5° grid cell as well as its impact on total electricity production at the country-scale.

The indicator for the amount of HP reduction at near-real-time, e.g. the month before the present month, is the relative reduction of HP during previous three months (HP3, see section 2.5) from the mean of HP during the respective three calendar months during the reference period, HP being simulated during the reference period with a temporally constant number of hydropower plants (V1) (compare Equation (6) and section 2.3). The HP relative reduction HPR3 is computed as

$$HPR3_t = Def_t / \overline{HP3_t} \tag{8}$$

How unusually low (or high) HP is as compared with normal conditions is can be quantified by apply the concept of standardized precipitation index (SPI) or the derived SSI that are both used in drought monitoring to quantifying how unusually low (or high) precipitation or streamflow. The attractive feature of thus a standardized index SHPI3 is that SPI is widely used for drought monitoring and the translation of the index values into different drought classes, such as mild or severe drought following Agnew (2000). A disadvantage is that a probability distribution function has to be fitted to the variable of interest, here HP3 (section 2.5), one for each calendar month. However, we found no suitable distribution function for HP3 (see section S2), possibly because HP3 is affected by reservoir operation limited by installed capacity. Therefore, nonparametric method that does not require to make assumptions about a probability distribution was used following Farahmand & AghaKouchak (2015). We relate each HP3 of a specific calendar month to an empirical non-exceedance probability F(HP3) using the Gringorten plotting position (Gringorten, 1963)

$$F(HP3) = \frac{k - 0.44}{n + 0.12} \tag{9}$$

where n is the sample size and k denotes the rank of HP3 in ascending order. Then we rescaled F(HP3) into a normalized probability, HP anomaly index HPA3, ranging between 0 (non-drought) and 1 (extreme drought), with

$$HPA3 = \frac{0.2 - F(HP3)}{0.2} \tag{10}$$

This normalization is consistent with the widely followed classification of Agnew

(2000) for SPI. If, for example, HP3 in May 2022 is a little less than the value that is not exceeded in only 1 out of 5 years (e.g. with a probability of 0.2 in each year), then a mild drought impact could be stated (Table 3). If $F(HP3) > 0.2$, the situation would not be considered to be a drought situation, and therefore qHP3 =0 even though there could be some HP reduction from normal.

HPA3 describes how unusually low HP is compared with normal and can be considered to be an HP anomaly indicator. The anomaly index HPA3 is easily understandable by decision makers and can be made transparent by relating it to the return periods listed in Table 3. Different form the relative reduction index HPR3, the HP anomaly index HPA3 assumes, like SPI and SSI, that the HP producers are used to the interannual variability of streamflow and related HP. For the same HP reduction, the anomaly index will show a relatively lower drought impact in grid cells with high interannual variability than in grid cells with low variability. The relationship between HPR3 and HPA3, as compared with SSI3, for three representative power plants are illustrated in Figure S8.

Table 3. Relationships of HP drought classes and HP anomaly index based on Agnew (2000)

Drought classes	Probability of non-exceedance F	Standardized drought index range	Return period (years)	HP anomaly HPA3
Extreme drought	0.02	Less than −2.00	50	0.9
Severe drought	0.05	Less than −1.65	20	0.75
Moderate drought	0.10	Less than −1.28	10	0.5
Mild drought	0.20	Less than −0.84	5	0
No drought	> 0.2	> −0.84	-	< 0

Combining the HP fraction to total electric generation r(HP) (Figure 1b), with the two HP drought indices result in two indices that describe the drought impact on total electricity production in a country. Electricity production relative reduction (EPR3) is the relative reduction of a national electricity production due to the streamflow drought impact on HP as compared with normal condition

$$\mathrm{EPR3} = r(HP) \cdot HPR3 \tag{11}$$

Similar to the EPR3, the electricity production anomaly EPA3 describes the effect of drought-related unusually low HP on total electricity production in a country, with

$$\mathrm{EPA3} = \sqrt{r(HP) \cdot HPA3} \tag{12}$$

Both indicators range between 0 (no drought impact) and 1 (extreme drought impact).

3.4.2. *Experimental Monitoring Results*

The ERA5 dataset (https://www.ecmwf.int/en/forecasts/datasets/reanalysis-datasets/era5) provides monthly atmospheric, land and oceanic climate variables within 3 months of real time and preliminary daily updates within 5 days of real time (Copernicus, 2017). Incorporating ERA5 meteorological reanalysis into WaterGAP would allow a timely simulation of the hydrological spatial-temporal dynamics. Then the proposed indices could be used to monitor and detect HP drought for any historical period after 1975 up to near-real time, thereby providing early warning information to stakeholders.

As near-real-time WaterGAP simulations using ERA5 are not yet possible, we illustrate potential HP drought monitoring indicators for the example month August 2003. Sample monitoring maps of SSI3, HPA3 and HPR3 for 0.5° grid cells worldwide are shown in Figure 8. The 2003 CEU drought is well captured as indicated by SSI3. Most EU countries were under hydrological drought. An obvious severe (to extreme) HP drought strip is identified across south France, Switzerland, Austria, and Slovakia in Europe. At the same time, Sweden, southeast China and part of Canada–United States border are found also under moderate to severe HP drought. The HPA3 index shows only a very small number of grid cells with a HP drought, as it only indicators cells as being at drought in which the probability of non-exceedance is lower than 0.2. In contrast, the HPR3 map shows all cells that suffer from any reduction during June-August 2003 from normal HP in June-August (Figure 8). HP reduction was mostly below 40% during this severe 2003 drought.

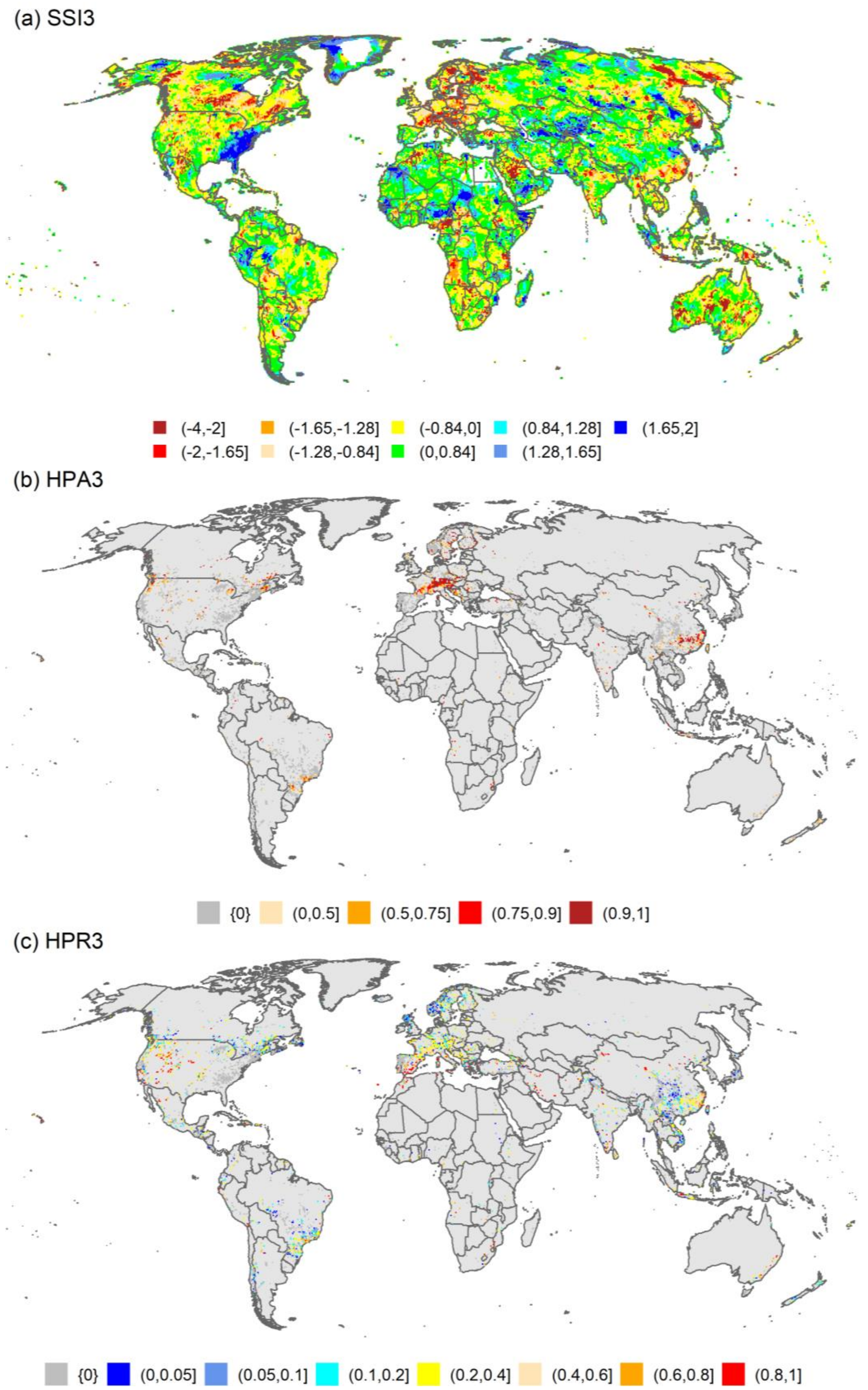

Figure 8. Illustrative maps of indicators of HP drought monitoring for the example of August 2003, when CEU experienced an extreme drought: Standardized Streamflow Index (SSI3) (a), HP anomaly (HPA3) (b), and HP relative reduction (HPR3) (c).

Classification of indicators was done according to Table 3. The white areas indicate grid cells with long-term average streamflow < 0.1 m^3/s.

Electricity production is managed for larger spatial aggregates such as countries. A monitoring system should therefore also provide spatially aggregated HP indicators. Figure 9 presents the country-level indicators of HP anomaly. The same level of HP anomaly might correspond to very different magnitudes of HP relative reduction for different countries, due to the differing interannual variability of HP. This underlies the necessity for multiple indicators.

Indicators of total electricity production anomaly give vital information about to what extent HP reduction during drought would adversely affect the whole electricity system. The extreme HP droughts in North America and CEU countries are degraded to mild/moderate droughts (Figure 10). Reduction of total electricity production in August 2003 was mostly less than 10%, except in Greenland and some African countries. Generally speaking, the abnormal climate in August 2003 had a significant impact on HP, especially in Europe and North America. Nevertheless, accounting for the HP contribution to electricity production, the negative impact becomes rather small. Please note that EPR3 and EPA3 do not indicate the total impact of drought on the electricity production in a country. It is likely larger as a lack of cooling water from thermal power plants may reduce their electricity production, too.

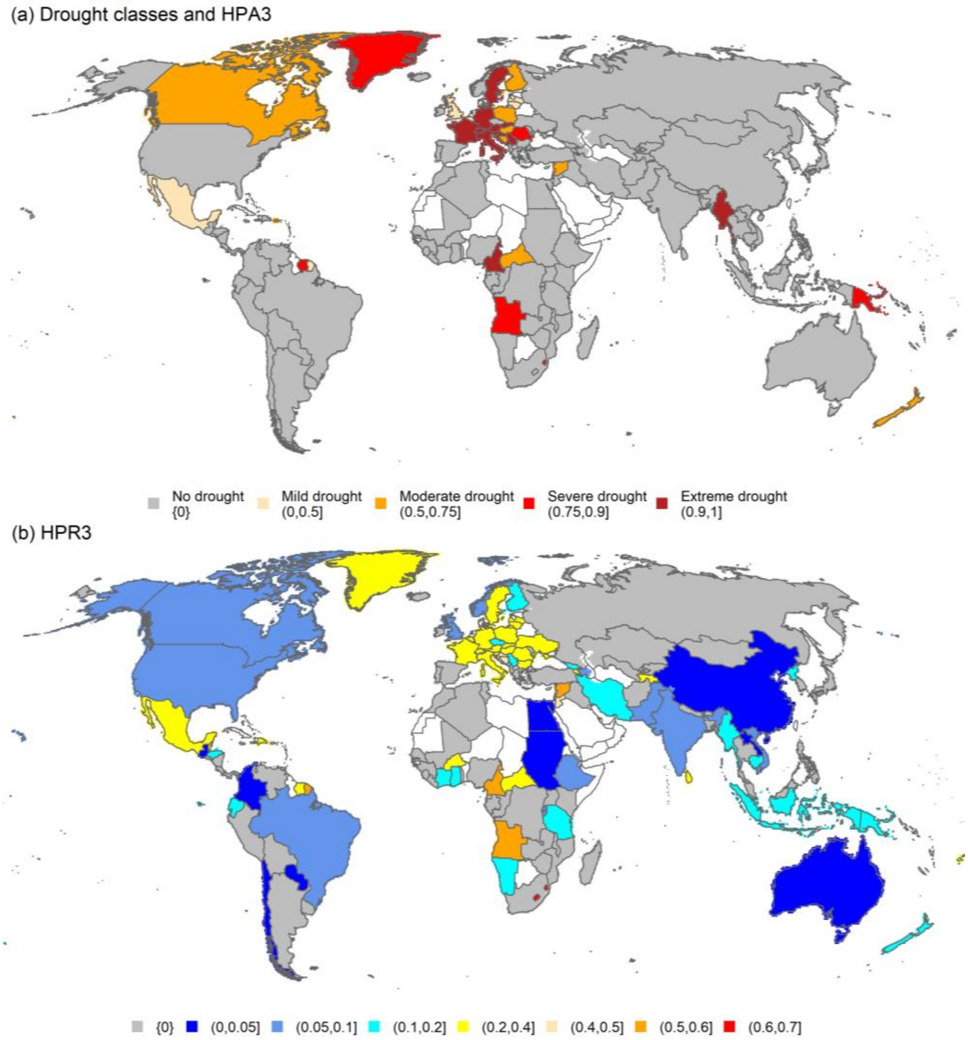

Figure 9. Country-level HP drought conditions as indicated by HP anomaly HPA3 (a), and HP relative reduction HPR3 (b) in August 2003.

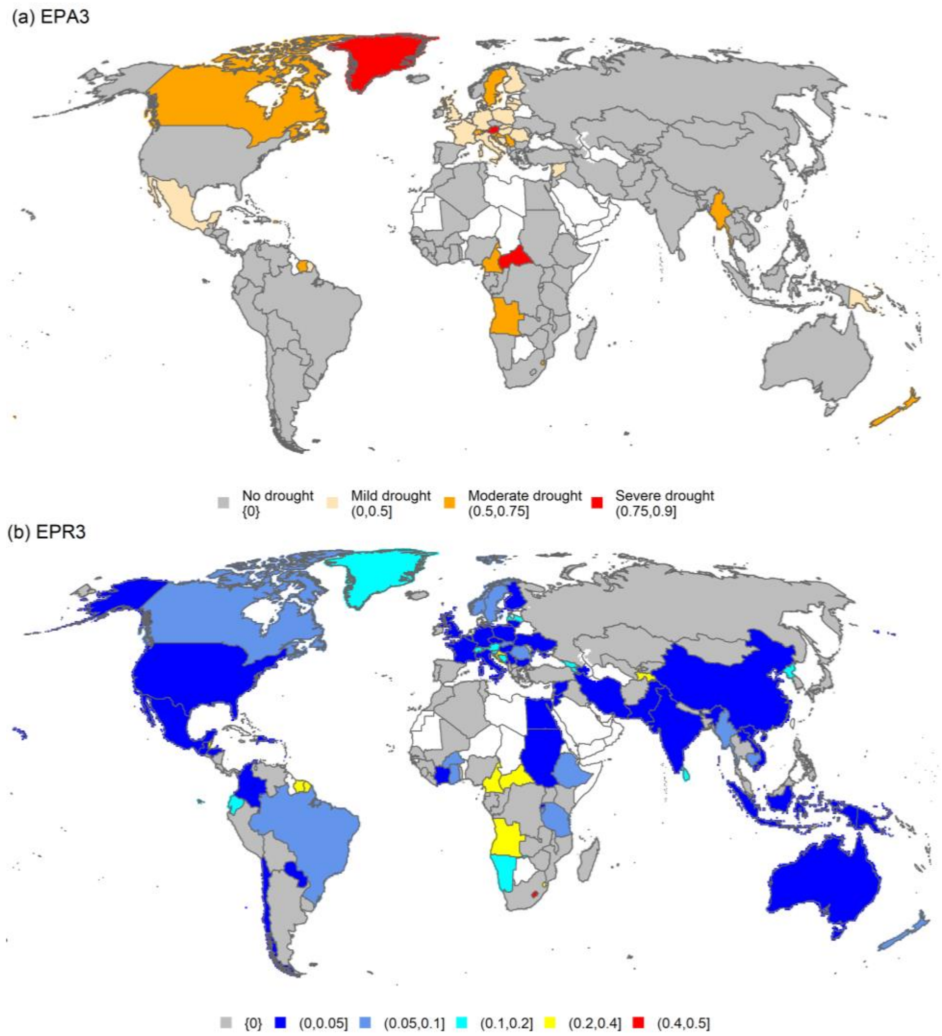

Figure 10. Country-level impact of drought on total electricity production (only due to drought impact on HP) as indicated by electricity production anomaly EPA3 (a) and relative reduction EPR3 (b) in August 2003.

4 Discussion

4.1. Uncertainties of Global-scale Simulation of HP

The HP model simulates the physical impact of changes in streamflow or outflow from reservoirs, while the socio-economic feedbacks from drought adaptation strategies, e.g. modification of electricity prices and demand-load portfolio, are not modelled. Furthermore, human alterations on streamflow, e.g. the estimation of water use, reservoir operation and related management, are unlikely to be fully simulated by

WaterGAP. Reservoir outflow discrepancies between modeled and observed are high due to a variety of reasons, including the erroneous inflow, uncertainty of operation algorithm and water use estimation (Döll et al., 2009). The impact of reservoir and water extraction on river flow regimes is certainly underestimated. The conflict between HP and other water users becoming more apparent during drought periods. In WGHM, reservoir-storage/streamflow is not allowed to fall below 10% of its capacity (Döll et al., 2009). However, human behavior is subject to more restrictions and frequent electricity trades (e.g. Jääskeläinen et al., 2018), whose impacts are difficult to measure worldwide. Therefore, unfortunately, even for the 705 WaterGAP reservoir plants, the uncertainties related to the simulated turbine release, reservoir storage, and thereby HP, cannot be overlooked. If we wish to improve such accuracy, refinement of the modeling of anthropogenic river flow alteration is urgently required in future research, and a thorough investigation of human component impacts during drought is suggested.

For all other hydropower plants except the 705 WaterGAP reservoir plants, we have no way of streamflow control in the HP model. Therefore, we assume constant hydraulic heads and steady flows, which is equivalent to the simulation monthly streamflow, to compute HP. In reality, the head varies as function of time. The value can differ substantially for high-elevation hydropower plants between wet and dry seasons, not to mention the dry and hot periods. The constant hydraulic head assumption suggests a degree of HP overestimation during dry periods, namely underestimated drought impact. The steady flow assumption suggests: (1) hydropower turbines run all day and night throughout the month, (2) the variance of turbine release within time step is small, and (3) all streamflow in river is diverted into the power plant. However, the short-term turbine broken and inspections happen from time to time, producing no electricity in those days. Furthermore, the actual turbine release is not time constant but varies dynamically between days, weeks, and seasons, particularly in the wet seasons, due to streamflow natural variations, plant regulation rules, flow constraints of the turbine, and changing electricity needs. To surmount these unavoidably uncertainties, we (1) used the $N_{installed}$ as upper boundary of power output (see Equation (1)), and (2) adopted a head reduction coefficient γ (see Equation (4)) for a better fit to HP statistics. And as only relative changes in HP are analyzed in this study, the uncertainties/errors due to the flow deviation are thus believed to be within acceptable limits.

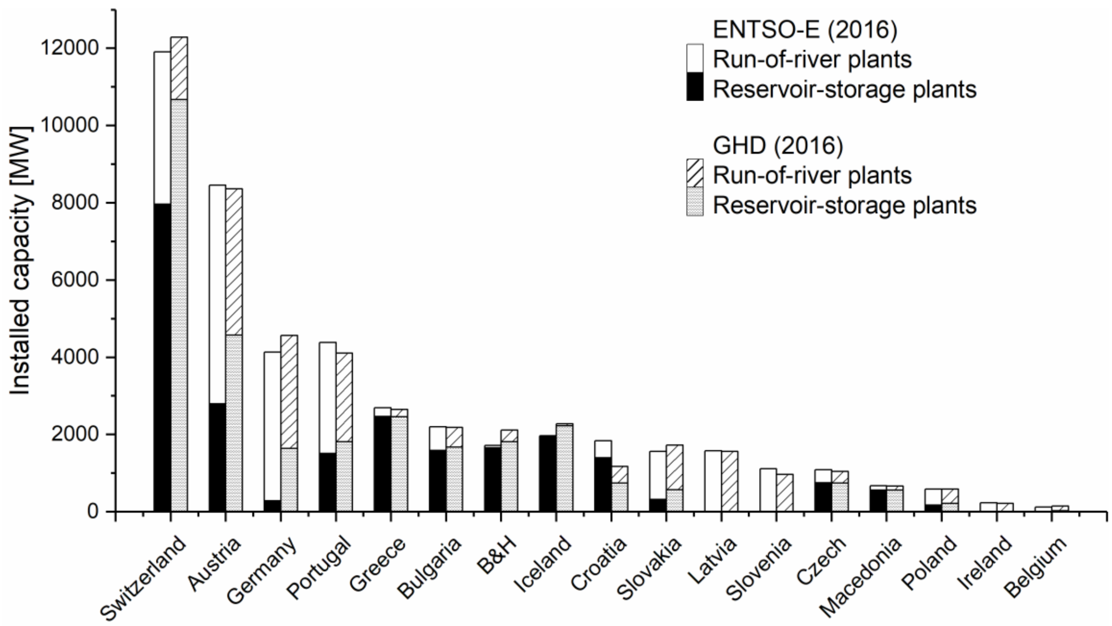

Figure 11. Comparison of installed capacities for some selected countries between

ENTSO-E statistics and the GHD database, distinguished for run-of-river and reservoir-storage plants (including all unknown category plants).

With respect to the run-of-river plants, we do not distinguish the algorithms for determining HP with reservoir-storage plants, due primarily to the limited number of identified categories (see Table S2). There are only 817 run-of-river plants are recognized with a total installed capacity accounting for 10.3%. While for Europe and North America, the plant category has probably been reported, it is believed that this is not possible for anywhere. We have compared the total installed capacities of run-of-river plants in some European countries with the ENTSO-E data (2017). A validation of the hydropower capacities per type as calculated from the GHD shows good overall agreement with the documented country values (Figure 11). Some run-of-river plants are categorized as reservoir-storage/unrecognizable plants due to the information deficits. The run-of-river plant is dramatically distinguished from the reservoir-storage plant because the former has limited or no storage, along with low hydraulic head. Therefore, the produced energy is heavily dependent on the natural streamflow available, generating much more power during wet season, and much less during drier and frozen months. The run-of-river hydropower has nearly constant hydraulic head and limited control of streamflow (Basso & Botter, 2012). From this perspective, the assumptions of head and flow made for computing HP are reasonable and closer to reality for run-of-river plants.

4.2. Future Electricity Demand from Hydropower

Electricity demand reflects human activities under socio-economical, technological and climatological drivers. In 2018, the energy demand worldwide grows by 2.3%, and the natural gas accounts for almost 45% of this growth. It is still crucial to accelerating the development of renewable energy, as countries strive to reduce carbon emission and air pollution from power generation. Given the flexibility and strong storage capacity of most hydropower plants, renewable energy from hydropower (including pumped hydro) provides the necessary backup to balance demand and supply. In recent years, the hydropower is developing with falling costs and improving performance. Nonetheless, hydroelectricity itself is vulnerable to climate as it strong-reliance on natural water resource and climate conditions. Climate change is projected to increase hydropower generation in some parts of the world and decrease it in others (Teotónio et al., 2017; Van Vliet et al., 2016a).

Water scarcity brings tremendous challenges to achieve sustainable development of energy security, especially during drought. While hydroelectricity supply may be deficit as a result of drought, the demand for electricity often increases due to the soaring requirements of air conditioning and water pumps. To cope with the severe unexpected hydropower failures, thereby keeping a cheap, stable and efficient electricity supply, the following strategies are recommended in the long run: (1) Finding and constructing more energy alternatives. In practice, the complementarity between hydro and coal, wind, solar, biomass or other energy sources is highly recommended, especially during periods of drought. Although this integration has already been implemented (Engeland et al., 2017), the expansion of the mix of multiple sources is expected in the context of technology development and transformation, and projected more powerful and frequent hydrological extremes in the near future. (2) Engaging hydroelectric development for countries with rich hydro resources. Developing more hydropower is of great importance to alleviate the energy crisis as well as avoid environmental contaminants. One evident example is China, which is affluent in hydro resources, but has rather low hydro development level. In 2005, the production of coal dominates the energy structure with more than 76.5% share, while hydropower only occupies less than 7% (Huang & Yan, 2009). However, over the last seven decades, its hydropower has risen more than 2,100-fold, to over 350 GW in 2018. The hydropower production in 2018 accounts for around 16.2%, rising to the second place, only after coal (CPMG, 2019). (3) Implementing quota-based water rights for more efficient water allocation. During drought, the water-use sectors of energy, water, food, health, and environment are often in intense competition. Water market and water reallocation systems play a significant role in balancing trade-offs between sectors and improving resilience to drought impact. It should be noted, however, as groundwater are an important environmental resource and provides strategic reserves against drought, an effective regulation of groundwater use is essential to ensuring sustainable water trading market (Culp et al., 2014).

5 Conclusions

In this study, a global hydropower database (GHD) was compiled. In comparison with EIA statistics, GHD has proven to be a relatively reliable and complete representation of global hydropower plants. A hydroelectricity production (HP) model was developed to simulate the monthly HP worldwide in 1975−2016 based on outputs of the global hydrological model WaterGAP. Reliability of the monthly streamflow simulated by WaterGAP was tested by comparing simulated values of the streamflow drought indicator SSI3 to observed values at 183 streamflow gauging stations. With a median NSE of 0.5, model performance can be regarded as moderate. The HP model can effectively represent the interannual variability of HP in countries as compared with EIA statistics. However, the impact of the 2003 Central European drought on HP is overestimated for 3 out of 8 countries.

A global drought risk analysis for the time period 1975−2016 showed that HP reductions of individual plants and 0.5° grid cells can range between 0 and 100% in 1 out of 10 years, while the respective reductions at the country scale show an equally large range of 4 to 93%. 20 out of 134 countries suffer from a reduction of more than 40%. Four indices, HPR3, HPA3, EPR3, and EPA3, are proposed to show drought impacts on HP in grid cells and total electricity production in countries in near-real-time global drought monitoring systems. These indicators may be computed in near-real-time with the HP model and inform the stakeholders such as hydropower producers or national energy agencies. There are two main advantages of these indices: (1) Depending on their preferences, stakeholders can either select the relative reduction index or the anomaly index; (2) As all indices range between 0 and 1, they can be easily comprehended and compared by stakeholders. Illustrative examples of global maps for monitoring HP drought impact suggest that the relative reduction indices are more informative than the anomaly indices as they reveal also smaller drought impacts and can be more easily grasped by stakeholders.

For the first time, a global risk map of HP reduction in 1 out of 10 years has been generated, different from the study of Van Vliet et al. (2016c) who only quantified HP in selected drought years. This is also the first time that indices suitable for monitoring drought impact on HP in near-real-time have been identified.

Author Contributions

WW and PD conceived the study. WW developed both the database and the HP model, performed the analyses and generated the figures. WW mainly wrote the manuscript supported by PD. EP carried out the K-S tests and provided hydrological inputs, while CH performed the streamflow comparisons. All authors provided critical feedback and helped shape the manuscript.

Acknowledgements

Part of the research was supported by the German Federal Ministry of Education and Research (BMBF) through its Global Resource Water (GRoW) funding initiative (GlobeDrought project, grant no. 02WGR1457B). This research was also funded by the National Key Research and Development Program of China (2016YFC0402203) and the National Natural Science Foundation of China (Grant No.91747208 and 51861125102). The global hydropower database (GHD) is freely available for

non-commercial use at https://doi.org/10.6084/m9.figshare.11283758.v3. The script of the HP model and the model inputs referred to in this paper, including global drainage direction map DDM30, WaterGAP model output, are also available at this figshare repository. Other datasets for this research can be addressed from World Power Plants Database (WPPD) (Global Energy Observatory, 2016), Global Power Plant Database (GPPD) (World Resources Institute, 2018), Global Reservoir and Dam Database (GRanD) version 2019 (Lehner et al., 2011), HydroSHEDS (Lehner et al., 2006), and International Energy Statistics (EIA, 2019), which have been appropriately cited.

References

Agnew, C. T. (2000). Using the SPI to Identify Drought. *Drought*, **12**(1), 29-42.

Ali, M. H., Alam, M. R., Haque, M. N., & Alam, M. J. (2012). Comparison of design and analysis of concrete gravity dam. *Natural resources*, **3**(01), 18-28.

Andreadis, K. M., Clark, E. A., Wood, A. W., Hamlet, A. F., & Lettenmaier, D. P. (2005). Twentieth-century drought in the conterminous United States. *Journal of Hydrometeorology*, **6**(6), 985-1001.

Bakis, R. (2007). The current status and future opportunities of hydroelectricity. *Energy Sources, Part B*, **2**(3), 259-266.

Basso, S., & Botter, G. (2012). Streamflow variability and optimal capacity of run‐of‐river hydropower plants. *Water Resources Research*, **48**(10).

Beames, P., Lehner, B., & Anand, M. (2019). Global Reservoir and Dam (Grand) Database. Technical Documentation, Version 1.3. edited.

Benejam, L., Saura Mas, S., Bardina, M., Solà, C., Munné, A., & García Berthou, E. (2016). Ecological impacts of small hydropower plants on headwater stream fish: from individual to community effects. *Ecology of Freshwater Fish*, **25**(2), 295-306.

Bonsal, B. R., Wheaton, E. E., Chipanshi, A. C., Lin, C., Sauchyn, D. J., & Wen, L. (2011). Drought research in Canada: A review. *Atmosphere-Ocean*, **49**(4), 303-319.

Bunn, S. E., & Arthington, A. H. (2002). Basic principles and ecological consequences of altered flow regimes for aquatic biodiversity. *Environmental Management*, **30**(4), 492-507.

Carrao, H., Naumann, G., & Barbosa, P. (2016). Mapping global patterns of drought risk: An empirical framework based on sub-national estimates of hazard, exposure and vulnerability. *Global Environmental Change*, **39**, 108-124.

Charpentier, A. (2011). On the return period of the 2003 heat wave. *Climatic Change*, **109**(3-4), 245-260.

Copernicus, C. C. S. C. (2017). ERA5: Fifth generation of ECMWF atmospheric reanalyses of the global climate, Copernicus Climate Change Service Climate Data Store (CDS). edited.

CPMG, C. P. M. G. (2019). China energy big data annual report (2019).

Culp, P. W., Glennon, R. J., & Libecap, G. (2014). *Shopping for water: How the market can mitigate water shortages in the American West*, Springer.

Department of Energy (Types of Hydropower Plants, https://www.energy.gov/eere/water/types-hydropower-plants.

Döll, P., & Lehner, B. (2002). Validation of a new global 30-min drainage direction map. *Journal of Hydrology*, **258**(1-4), 214-231.

Döll, P., Fiedler, K., & Zhang, J. (2009). Global-scale analysis of river flow alterations due to water withdrawals and reservoirs. *Hydrology and Earth System Sciences*, **13**(12), 2413-2432.

Döll, P., Müller Schmied, H., Schuh, C., Portmann, F. T., & Eicker, A. (2014). Global‐scale assessment of groundwater depletion and related groundwater abstractions: Combining hydrological modeling with information from well observations and GRACE satellites. *Water Resources Research*, **50**(7), 5698-5720.

Dracup, J. A., Lee, K. S., & Paulson, E. G. (1980). On the definition of droughts. *Water Resources Research*, **16**(2), 297-302.

EIA (2019). U.S. Energy Information Administration independent statistics and analysis, https://www.eia.gov/beta/international/data.

El-Hawary, M. E., & Christensen, G. S. (1979). *Optimal economic operation of electric power systems*, Academic Press New York.

Engeland, K., Borga, M., Creutin, J., François, B., Ramos, M., & Vidal, J. (2017). Space-time variability of climate variables and intermittent renewable electricity production ‐ A review. *Renewable and Sustainable Energy Reviews*, **79**, 600-617.

ENTSOE (Statistical Factsheet 2016, https://docstore.entsoe.eu/Documents/Publications/Statistics/Factsheet/entsoe_sfs_2016_web.pdf.

Farahmand, A., & AghaKouchak, A. (2015). A generalized framework for deriving nonparametric standardized drought indicators. *Advances in Water Resources*, **76**, 140-145.

Global Energy Observatory (World Power Plants Database, https://datasource.kapsarc.org/explore/dataset/world-power-plants-list/.

Golombek, R., Kittelsen, S. A., & Haddeland, I. (2012). Climate change: impacts on electricity markets in Western Europe. *Climatic Change*, **113**(2), 357-370.

Gringorten, I. I. (1963). A plotting rule for extreme probability paper. *Journal of Geophysical Research*, **68**(3), 813-814.

Hambling, D. (2020). Hydro power falters in persistent drought, https://www.theguardian.com/news/2016/mar/30/weatherwatch-hambling-venezuela-hydroelectric-dam-guri-dry-reservoirs-colombia?utm_content=buffer2ce55&utm_medium=social&utm_source=twitter.com&utm_campaign=buffer.

Hänggi, P., & Weingartner, R. (2012). Variations in discharge volumes for hydropower generation in Switzerland. *Water Resources Management*, **26**(5), 1231-1252.

Haslinger, K., & Blöschl, G. (2017). Space ‐ time patterns of meteorological drought events in the European Greater Alpine Region over the past 210 years. *Water Resources Research*, **53**(11), 9807-9823.

Herrera-Estrada, J. E., Diffenbaugh, N. S., Wagner, F., Craft, A., & Sheffield, J. (2018). Response of electricity sector air pollution emissions to drought conditions in the western United States. *Environmental Research Letters*, **13**(12), 124032.

House, C., Way, S. N., & Sutton, L. (2018). The world's water battery: Pumped hydropower storage and the clean energy transition, United Kingdom.

Huang, H., & Yan, Z. (2009). Present situation and future prospect of hydropower in China. *Renewable and Sustainable Energy Reviews*, **13**(6-7), 1652-1656.

IEA (2019). International Energy Agency: Hydropower Tracking Clean Energy Progress, https://www.iea.org/tcep/power/renewables/hydropower/.

IHA, I. H. A. (2018). 2018 Hydropower status report, London, United Kingdom.

IPCC (2014). The physical science basis. Contribution of working group I to the fifth assessment report of the intergovernmental panel on climate change. *K., Tignor, M., Allen, SK, Boschung, J., Nauels, A., Xia, Y., Bex, V., Midgley, PM, Eds*, 1535.

Jääskeläinen, J., Veijalainen, N., Syri, S., Marttunen, M., & Zakeri, B. (2018). Energy security impacts of a severe drought on the future Finnish energy system. *Journal of Environmental Management*, **217**, 542-554.

Laaha, G., Gauster, T., Tallaksen, L., Vidal, J., & Stahl, K., et al. (2017). The European 2015 drought from a hydrological perspective. *Hydrology and Earth System Sciences*, **21**, 3001-3024.

Lehner, B., Verdin, K., & Jarvis, A. (2006). HydroSHEDS technical documentation, version 1.0. *World Wildlife Fund US, Washington, DC. Available at http://hydrosheds.cr.usgs.gov.*, 1-27.

Lehner, B., Liermann, C. R., Revenga, C., Vörösmarty, C., & Fekete, B., et al. (2011). High‐resolution mapping of the world's reservoirs and dams for sustainable river‐flow management. *Frontiers in Ecology and the Environment*, **9**(9), 494-502.

Liu, Y., Zhu, Y., Ren, L., Singh, V. P., & Yong, B., et al. (2019). Understanding the Spatiotemporal Links Between Meteorological and Hydrological Droughts From a Three‐Dimensional Perspective. *Journal of Geophysical Research: Atmospheres*, **124**(6), 3090-3109.

Masih, I., Maskey, S., Mussá, F., & Trambauer, P. (2014). A review of droughts on the African continent: a geospatial and long-term perspective. *Hydrology and Earth System Sciences*, **18**(9), 3635-3649.

Meza, I., Siebert, S., Döll, P., Kusche, J., & Herbert, C., et al. (2019). Global-scale drought risk assessment for agricultural systems. *Nat. Hazards Earth Syst. Sci*.

Mukheibir, P. (2013). Potential consequences of projected climate change impacts on hydroelectricity generation. *Climatic Change*, **121**(1), 67-78.

Müller Schmied, H., Eisner, S., Franz, D., Wattenbach, M., Portmann, F. T., Flörke, M., & Döll, P. (2014). Sensitivity of simulated global-scale freshwater fluxes and storages to input data, hydrological model structure, human water use and calibration. *Hydrology and Earth System Sciences*, **11**(2), 1583-1649.

Müller Schmied, H., Adam, L., Eisner, S., Fink, G., & Floerke, M., et al. (2016). Variations of global and continental water balance components as impacted by climate forcing uncertainty and human water use. *Hydrology and Earth System Sciences*, **20**(7), 2877-2898.

Schewe, J., Gosling, S. N., Reyer, C., Zhao, F., & Ciais, P., et al. (2019). State-of-the-art global models underestimate impacts from climate extremes. *Nature Communications*, **10**(1), 1005.

Schill, W., & Kemfert, C. (2011). Modeling strategic electricity storage: the case of pumped hydro storage in Germany. *The Energy Journal*, 59-87.

Singh, S. C., & Sally, M. (2020). Electricity supply to face disruptions amid high demand and acute water shortage

,

https://economictimes.indiatimes.com/industry/energy/power/electricity-supply-to-face-disruptions-amid-high-demand-and-acute-water-shortage/articleshow/51675775.cms.

Smith, R. L. (1984). Threshold methods for sample extremes, edited, pp. 621-638, Springer.

Spinoni, J., Naumann, G., Vogt, J. V., & Barbosa, P. (2015). The biggest drought events in Europe from 1950 to 2012. *Journal of Hydrology: Regional Studies*, **3**, 509-524.

Teotónio, C., Fortes, P., Roebeling, P., Rodriguez, M., & Robaina-Alves, M. (2017). Assessing the impacts of climate change on hydropower generation and the power sector in Portugal: a partial equilibrium approach. *Renewable and Sustainable Energy Reviews*, **74**, 788-799.

UNCTAD (2017). The Least Developed Countries Report 2017, United Nations Conference on Trade and Development.

Van Vliet, M., van Beek, L., Eisner, S., Flörke, M., Wada, Y., & Bierkens, M. (2016b). Multi-model assessment of global hydropower and cooling water discharge potential under climate change. *Global environmental change*, **40**, 156-170.

Van Vliet, M. T., Wiberg, D., Leduc, S., & Riahi, K. (2016a). Power-generation system vulnerability and adaptation to changes in climate and water resources. *Nature Climate Change*, **6**(4), 375.

Van Vliet, M. T., Sheffield, J., Wiberg, D., & Wood, E. F. (2016c). Impacts of recent drought and warm years on water resources and electricity supply worldwide. *Environmental Research Letters*, **11**(12), 124021.

Vicente-Serrano, S. M., López-Moreno, J. I., Beguería, S., Lorenzo-Lacruz, J., Azorin-Molina, C., & Morán-Tejeda, E. (2011). Accurate computation of a streamflow drought index. *Journal of Hydrologic Engineering*, **17**(2), 318-332.

Wan, W., Wang, H., & Zhao, J. (2020). Hydraulic potential energy model for hydropower operation in mixed reservoir systems. *Water Resources Research*, e2019W-e26062W.

World Resources Institute (2020). Global Power Plant Database. Published on Resource Watch and Google Earth Engine, http://datasets.wri.org/dataset/globalpowerplantdatabase.

Zaherpour, J., Gosling, S. N., Mount, N., Schmied, H. M., & Veldkamp, T. I. E., et al. (2018). Worldwide evaluation of mean and extreme runoff from six global-scale hydrological models that account for human impacts. *Environmental Research Letters*, **13**, 65015.

Zhang, L., & Zhou, T. (2015). Drought over East Asia: a review. *Journal of Climate*, **28**(8), 3375-3399.

Zhao, T., Zhao, J., & Yang, D. (140). Improved dynamic programming for hydropower reservoir operation, .

Zhou, Z. (1997). *Water resources and hydropower planning*, China Water and Power Press (in Chinese).